journal

J. Am. Ceram. Soc., 77 [6] 1613–23 (1994)

Molten Glass Corrosion Resistance of Immersed Combustion-Heating Tube Materials in Soda–Lime–Silicate Glass

S. Kamakshi Sundaram,* Jen-Yan Hsu,* and Robert F. Speyer*

School of Materials Science and Engineering, Georgia Institute of Technology, Atlanta, Georgia 30332-0245

The corrosion resistance of molybdenum, molybdenum disilicide, and a $SiC_{(p)}/Al_2O_3$ composite to molten soda–lime–silicate glass was studied. The ASTM-C621-84 corrosion test method was modified because of inherent inaccuracies in the method and Si attack of platinum crucibles. Specimen-glass interfacial regions were characterized using XRD, SEM, and EDS. After 48 h of exposure at 1565°C, the half-down corrosion recessions of Mo, $MoSi_2$, and $SiC_{(p)}/Al_2O_3$ were 0.11, 0.316, and 0.26 mm, respectively. Mo oxidized to form a MoO_2 surface scale which cracked, allowing glass seepage and further oxidation. Silicon was leached out of $MoSi_2$ into the glass, leaving a Mo_5Si_3 interface and particles of Mo near the interface. For the $SiC_{(p)}/Al_2O_3$ composite, bubbles observed at the interfacial regions formed from oxidation of SiC to form CO. Thermodynamic modeling corroborated these experimental observations.

I. Introduction

THE work discussed herein is part of a larger research thrust to develop materials for immersed gas-fired radiant burner tubes for glass melters. In the evaluation of candidate materials, our research has adopted a parallel approach, separately evaluating molten glass corrosion, combustion gas corrosion, as well as using thermodynamic simulations for both processes. Gas corrosion investigations are reported elsewhere.[1,2] In the present paper, the molten glass corrosion behavior of candidate materials is presented.

A selection of the candidate materials which were evaluated and the results of which are presented herein are the following: molybdenum, molybdenum disilicide, and $SiC_{(p)}/Al_2O_3$ composite (p refers to particulate). Molybdenum has been used as the electrode material for electric melting and boosting in glass melting tanks for many years.[3,4] Molybdenum disilicide has demonstrated a self-protective mechanism of forming a protective SiO_2 layer at the surface in an oxidizing atmosphere.[5] For temperatures below 600°C, oxidation of molybdenum disilicide forms solid MoO_3 and SiO_2 products on the surface. The formation of $MoO_{3(s)}$ in microcracks extends them and ultimately the solid fragments into powder, referred to as $MoSi_2$ pest.[6] In the case of $SiC_{(p)}/Al_2O_3$ composite, the combination of high thermal conductivity of SiC and the refractory properties of Al_2O_3 were expected to make it potentially suitable for the combustion product side of the present application. The composite is fabricated by the Lanxide process:[7] directed oxidation of molten aluminum infiltrating into a particulate SiC matrix. Fused-cast AZS (50.8 wt% alumina, 32.6 wt% zirconia, 14.9 wt% silica, plus impurity phases), used as molten glass container material in this investigation, is well known for its corrosion resistance to molten glass[8–10] and is a common commercial glass tank refractory.

Bockris and co-workers[11] used molybdenum crucibles to study the interaction of Mo with molten binary silicates and detected a 0.15 wt% molybdenum absorption as MoO_3 by molten Na_2O–SiO_2 at 1750°C after 3 h in a H_2–N_2 atmosphere. Minute reaction between pure silica and Mo under vacuum at 1600°C has also been observed.[12] Soda–lime–silicate glass, free of iron and sulfur, has been shown to be only very slightly corrosive toward molybdenum in the temperature range 1000° to 1300°C in an oxidizing atmosphere.[13] The slight observed corrosion was due to reaction with dissolved oxygen, postulated (though not shown experimentally) to form MoO_3.[14]

The oxygen solubility of a glass melt is not governed entirely by the oxygen partial pressure of the furnace atmosphere; basicity,[15] e.g., the concentration of alkali, and the concentration and type of polyvalent species present in the melt[16,17] are also controlling factors. Based on solubility measurements of $CO_{2(g)}$ in glass, Pearce[18] showed that oxygen ion activity increased dramatically with increasing alkali content in sodium silicate glasses. Because of its open structure, however, oxygen is predominantly absorbed molecularly rather than atomically.[19]

Oxidation of molybdenum by dissolved oxygen in pure soda–lime–silicate glass melts was minute as compared to melts containing 0.1 wt% Fe and 0.3 wt% SO_3. On reacting with Na_2SO_4, MoS_2 formed by

$$3Mo_{(s)} + 2Na_2SO_{4(s)} = MoS_{2(s)} + 2Na_2MoO_{4(s)}$$

The addition of 0.10% Fe_2O_3 only (no sulfur compounds) to the soda–lime–silicate melt did not show any appreciable corrosion.[14] Ooka[13] studied the effect of the amount of As_2O_3, Na_2SO_4, and Sb_2O_3 present in soda–lime–silicate glass on the weight loss of molybdenum at 1500°C for 50 h. As_2O_3 additions were found to be highly corrosive to Mo, Na_2SO_4 was found to be slightly corrosive (forming MoS_2), and Sb_2O_3 had no effect. Lead-containing glasses were highly corrosive to Mo. Pecoraro *et al.*[20] observed that the extent of corrosion by the mechanism of direct elemental solubility was negligibly small; corrosion proceeded primarily through the oxidation of the metal caused by oxidizing agents, dissolved oxygen and water, or a melt constituent which could accept electrons from the metal. Literature studies do not clearly indicate the form of corrosion product nor were they able to accurately measure corrosion rates.

Muan and Spear[21] evaluated thermodynamic calculations for the systems Mo–O, Mo–Si–O, and Na_2O–CaO–SiO_2 and suggested $MoSi_2$ as a potentially suitable material for gas boosters immersed in glass melting tanks. No experimental evidence of the corrosion rate or mechanism has been reported. The corrosion resistance of $SiC_{(p)}/Al_2O_3$ composite in molten glass has also not been reported. However, the corrosion resistance of pure alumina has been studied extensively[22–26] and shown to be less than optimum.

II. Experimental Procedure

(1) Corrosion Testing

The ASTM standard method C621-84 for isothermal corrosion resistance of refractories to molten glass was initially

J. Smialek—contributing editor

Manuscript No. 194696. Received April 12, 1993; approved February 16, 1994. Supported by the Gas Research Institute under Contract No. 5090-298-2073.

partial immersion of a test specimen of rectangular or circular cross section in molten glass contained in a Pt crucible. The recession from original material dimensions at the glass line and at an immersed position are measured after high-temperature exposure for various periods of time. Modifications of the standard were made based on the following encumbrances: (i) molybdenum oxidizes and volatilizes above the glass line at temperatures exceeding ~600°C, and (ii) silicon dissolves into the melt from the $MoSi_2$ and $SiC_{(p)}/Al_2O_3$ test coupons, and in turn alloys with the platinum crucible to form low-temperature eutectic phases, destroying the crucible.

The Pt crucible as specified in ASTM C621-84 was replaced by an AZS (UNICOR501, Corhart Refractories Corp.) crucible with a containment volume of 3.81-cm diameter by 3.81-cm depth to contain molten glass. The choice of AZS was made after static corrosion testing of fusion-cast AZS, MgO-partially-stabilized zirconia (PSZ) (Coors Ceramics Co., Golden, CO), fusion-cast chromia (Carborundum Co., Monofrax Refractories Division, Falconer, NY), and bonded chromia (Corhart Refractories Corp., Buchannon, WV) by following the ASTM C621-84 standard. The results of corrosion testing, presented in Figs. 1(a) and (b), indicate that AZS was the least corroded material at both the glass-line and half-down regions.

The soda–lime–silicate glass (Owens-Illinois, Inc.) used in the present investigation is a common container-glass composition. A chemical analysis of the as-received glass in weight percent shows 73.3% SiO_2, 13.3% Na_2O, 11% CaO, 1.5% Al_2O_3 0.3% K_2O, 0.2% MgO, 0.2% SO_3, 0.2% ZrO_2, and 0.07% Fe_2O_3. Molybdenum (Johnson Matthey/AESAR) specimens were of 12.5-mm diameter by 12.5-mm length for the purpose of complete immersion. Chemical analysis for trace elements in as-received molybdenum showed less than 1 ppm of Al, Ca, Cr, Cu, Mg, Mn, Ni, Pb, Si, Sn, and Ti, less than 2 ppm of C and O, and less than 14 ppm of Fe. Cylindrical specimens of $MoSi_2$ (Kanthal Super 33, Kanthal Corp.) and $SiC_{(p)}/Al_2O_3$ (Du Pont Lanxide Composites) of 12.5-mm diameter by 60-mm length were used. The as-received $MoSi_2$ contained 1.7 vol% Mo_5Si_3 grains, generally in contact with amorphous aluminosilicate glassy pockets comprising 18.6 vol% of the specimen, as determined by scanning electron microscopy image analysis.

The test configuration is sketched in Fig. 2. The quantity of glass powder put into the AZS crucible was adjusted so that a molten glass level of 18.8 mm was maintained. The as-received glass was crushed to −40 mesh, and the AZS crucible with 48.5 g of glass was placed inside an electrically heated furnace. The glass was heated to 1565°C and allowed to equilibrate at

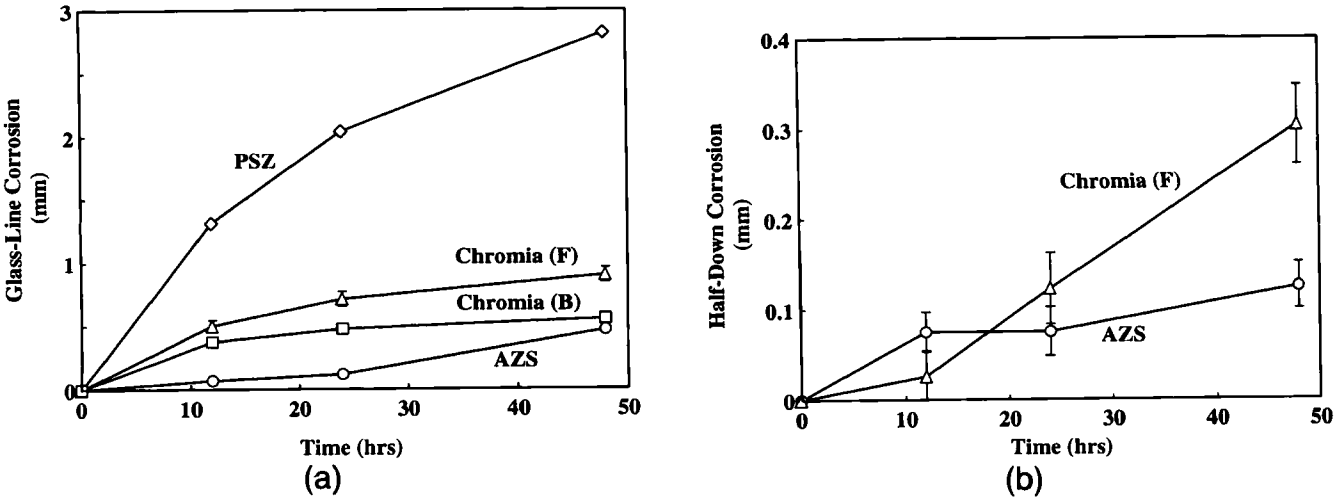

Fig. 1. Corrosion rate of refractory containment materials at (a) glass-line and (b) half-down regions. The error bars indicate the standard deviation in the measurement of specimen diameters before the corrosion tests. These out-of-roundness deviations represent the largest errors of all contributions to error in the measurement.

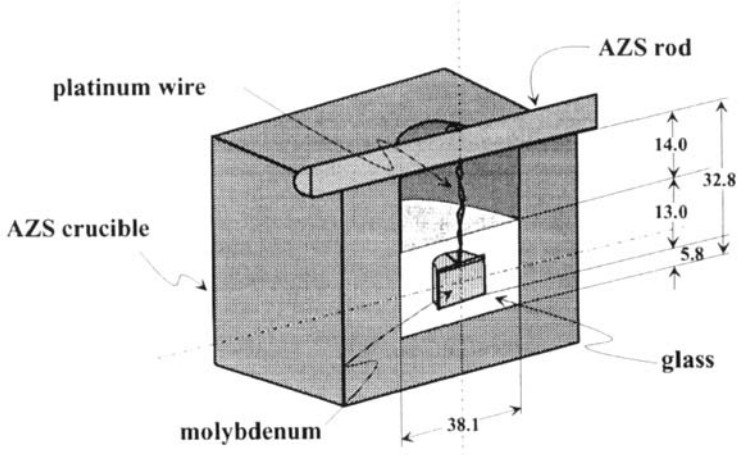

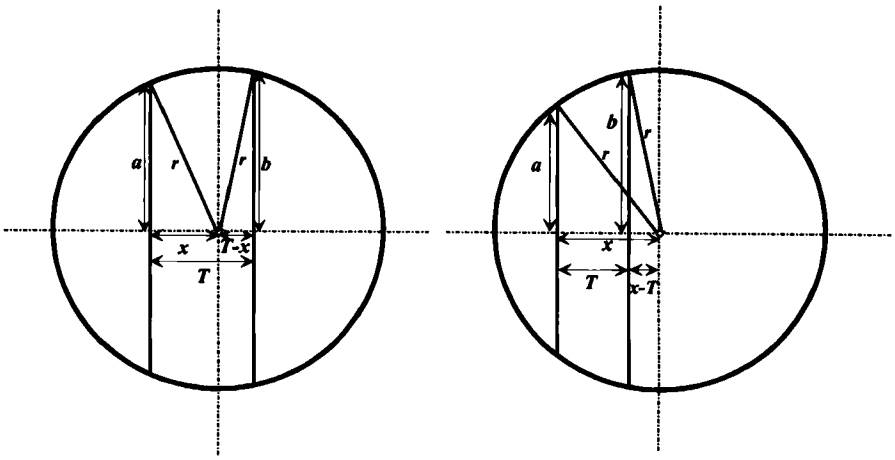

Fig. 3. Correlation of measured diameters $2a$ and $2b$ to the true diameter $2r$ of the corroded specimen, for a known blade thickness T. Left: case where blade cuts through the center. Right: case where blade misses the center.

that temperature for 2 h to obtain bubble-free glass. Test specimens were then loaded into the crucible.

The diameters of the pre-exposed specimens at the glass-line as well as the half-down positions were measured using digital vernier calipers (Mitutoyo Corp., Model CD-8″) with a precision of ±0.01 mm. Each specimen was rotated and the measurement was performed at 10 points of contact at the two positions. The standard deviation of measured diameters ranged from 0.0052 to 0.0255 mm. The planeness and parallelness of the surfaces of the specimens were checked using a machinist's square. If the faces were not truly flat and perpendicular to the cylindrical axis, they were ground using 600-μm polishing paper and checked again until they were flat. In the case of molybdenum specimens, the center was marked using a lathe (Rivett Lathe and Grinders Inc., Boston, MA) and a self-centering collet before the corrosion test (precision: ±0.051 mm).

$MoSi_2$ and $SiC_{(p)}/Al_2O_3$ specimens were affixed to zircon support wafers with zircon cement and allowed to dry overnight. They were preheated to 1000°C and maintained at that temperature for 10 min, to avoid specimen thermal shock when transferred to the equilibrated molten glass. Each molybdenum specimen in a Pt wire basket was suspended by Pt wire into the molten glass so that the specimen was completely immersed. These specimens were quickly immersed in the molten glass at the test temperature; they were not preheated so as to avoid atmospheric oxidation. The durations of corrosion tests were 12, 24, and 48 h at 1565°C in static air. The test temperature of 1565°C corresponds to the hot-spot temperature in a commercial glass tank. One specimen was tested for each experimental condition. After exposure, the specimens were removed from the melt and allowed to cool in ambient.

The corroded specimen rods were cut lengthwise along the rod axis using a diamond wafering blade (Buehler, Lake Bluff, IL) with a thickness of 0.34 ± 0.1 mm (±0.1 mm positioning precision). Several initial steps were taken to ensure that the wafering blade propagated through the center of the specimen: For Mo after exposure, the top Mo surface was ground until a flat surface was exposed, while for other specimens, the uncorroded top surface was already exposed. The specimens were then mounted on this surface using thermal glue (Buehler). A cut running parallel to the axis of each specimen was made. The edges along this side face were checked as to whether they were parallel to each other using a digital vernier calipers. If they were not parallel, the side face was repeatedly ground with uneven pressure, and remeasured, until they were parallel; this while for Mo, the center was previously marked (see above). The specimens were then mounted on the side face, and another cut was made through the marked center, down the center axes of the specimens.

The diameters at the glass-line and half-down positions on the cut surfaces were measured using the platform and microscope of a micro-hardness tester (Model HMV 2000, Shimadzu Co., Kyoto, Japan) where the precision of diameter measurement was ±0.01 mm. An oil of refractive index of 1.51 was used to cause the glass to vanish from view so that the interface could be clearly seen through the microscope.

The ASTM C621-84 procedure does not account for the thickness of the cutting blade when evaluating cylindrical specimens; it specifies only to determine the average of the measured diameters of the specimen halves. Figure 3 illustrates the effect of blade thickness on the corrosion measurement. If $2a$ and $2b$ are the measured diameters, and $2r$ the genuine diameter of the specimen, then r can be calculated:

$$r = \pm\left[\left(\frac{b^2 + T^2 - a^2}{2T}\right)^2 + a^2\right]^{1/2}$$

where T is the thickness of the blade. The calculated propagated error by using the equation of r ranged from 0.0003 to 0.007 mm. The computational procedure is elaborated upon elsewhere.[28] Since the calculated errors corresponded to less than the y-axis dimension of data markers, error bars for radius recession plots are not shown.

The reaction of the AZS container with molten glass was separately evaluated. A 48.5-g sample of glass was placed in an AZS container and maintained at 1565°C. After equilibration, a small quantity of the melt was removed from the center of the exposed melt surface using a Pt boat, and quenched after 3, 6, 12, 24, 36, and 48 h of reaction with the container. These samples were then chemically analyzed for SiO_2, Al_2O_3, and ZrO_2.

(2) Characterization

The glass–specimen interface was characterized using scanning electron microscopy (SEM) (Model 1810, AMRAY, Bedford, MA). Cross sections of specimens were mounted in epoxy and the surfaces were ground smooth using 120-, 240-, 320-, 400-, and 600-grit abrasive papers and then polished with diamond paste (30, 15, 6, and 1 μm). The polished samples were etched in 1% HF for ~30 s, rinsed with distilled water, and then cleaned in an ultrasonic cleaner using distilled water, and dried.

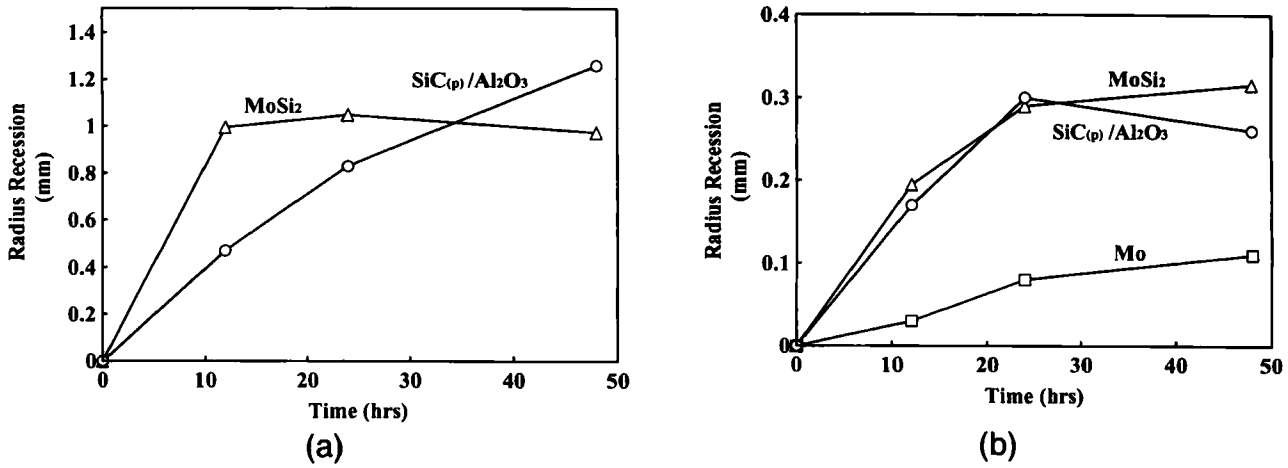

Fig. 4. Specimen recessions at (a) glass-line and (b) half-down regions when exposed to soda–lime–silicate glass at 1565°C.

TS16-J018, Princeton Gamma Technology, Princeton, NJ) to establish the chemistry at and across the interfacial regions.

A 48-h corrosion test was repeated using a specimen with a semicircular cross section where the flat interface was for the convenience of XRD analysis. Diffraction patterns were taken on the glass-coated surface and then repeated after grinding the flat surface with 600-μm abrasive paper for 10 min and cleaning. This process was continued until the interface was exposed and then penetrated. The specimen was analyzed using a computer-interfaced (Model VAX-11/730, Digital Equipment Co., Northboro, MA) X-ray (Cu$K\alpha$) powder diffractometer (Model 12045 X-ray diffraction unit, Philips Electronic Instruments Co., Mount Vernon, NY) with a 1-s time constant and 0.02° step size over a 2θ range of 20–80°. Using a computer search program, the X-ray diffraction patterns were matched to JCPDS data and corresponding phases were identified. In the phase identification procedure (D5000, Alfred University X-ray Laboratory, Alfred, NY), two types of searches, LIST and SUBTRACT, were used. The LIST search performed a forced match of the input data with the entire JCPDS powder diffraction file and produced a list of potential matches. The SUBTRACT search performed a Hanawalt search and subtracted a matching compound that met a figure-of-merit criterion.

(3) Thermodynamic Analysis

Thermodynamic analysis of Mo–O, Mo–Si–O, Si–C–O, and Al–O systems were performed to predict solid–molten glass interfacial chemistry. The standard-state free energies of reaction, forming MoO_2, MoO_3,[29,30] Mo_3Si, and Mo_5Si_3, and $CaMoO_4$[31] were computed and plotted against temperature (Ellingham diagrams). Thermodynamic data were obtained from the Facility for the Analysis of Chemical Thermodynamics (F*A*C*T).[7] These thermodynamic plots represent equilibria among solids and molecular oxygen in their standard states, that is, pure oxygen at 1 atm and pure solids.

Since oxygen dissolves predominantly molecularly in glass,[19] the chemical potential of O_2 in molten glass is equal to that in the furnace (electrically heated) atmosphere, where $p_{O_2} \cong 0.2$. The activities of oxygen in the glass and in the atmosphere, however, are not equal, since soluble gas is generally considered as a dilute solution which is non-Raoultian. Norton[32] has determined that the ratio of the concentration of molecular oxygen in the glass relative to that in the furnace atmosphere at 1078°C is 0.01. The "coefficient of solubility" does not change appreciably with temperature.[19,32] Thus, the Henrian activity of molecular oxygen in glass was taken to be 2×10^{-3}, and Richardson lines corresponding to this oxygen activity are drawn on the Ellingham diagrams.

III. Results and Discussion

The chemical analyses of the glass (removed from the top-center of the melt) after interaction with AZS for varying times are shown in Table I. No significant changes in these constituents were observed up to 12 h of exposure. Beyond 12 h, Al_2O_3 and ZrO_2 concentration gradually increased. After 48 h of exposure, the Al_2O_3 content increased to 2.8%, and the ZrO_2 content to 0.15%. The effect of this compositional change on the specimen corrosion rate is not known. Replenishing glass melt after every 12 h of exposure was considered and rejected since it changes the present static testing to a semidynamic corrosion test.[28]

Figures 1(a) and (b) show the glass-line and half-down recessions, respectively, of potential containment materials. In the case of the glass-line corrosion, AZS was the least corroded material. In the case of the half-down region, initially fusion-cast chromia showed a corrosion rate less than that of AZS, but increased steeply beyond 12 h of exposure. Chromia also severely discolored the glass. The half-down corrosion rates of bonded chromia and PSZ could not be measured because of specimen cracking.

Figures 4(a) and (b) show the glass-line and half-down recessions of cylindrical specimens (in turn contained in AZS crucibles), respectively, by molten glass. In the case of glass-line corrosion, $SiC_{(p)}/Al_2O_3$ showed a corrosion rate initially less than that of $MoSi_2$ but showed greater recession rates after 12 h of exposure, and was the most corroded specimen after 48 h of exposure. With regard to half-down corrosion, Mo was the least corroded material. $MoSi_2$ and $SiC_{(p)}/Al_2O_3$ showed similar corrosion behavior. The indicated downward trend for $SiC_{(p)}/Al_2O_3$ could not be corroborated by repeated testing because of specimen availability.

(1) Molybdenum

Figure 5 shows XRD patterns starting from the glass side, penetrating through the interface. On the glass side, only one crystalline peak is apparent, which matches with $CaMoO_4$. This

Table I. Chemical Analysis of Glass after Interactions with AZS Crucibles at 1565°C

Corrosion time (h)	Composition (wt%)		
	SiO_2	Al_2O_3	ZrO_2
0	73.3	1.5	0
3	72.6	1.4	0
6	72.8	1.4	0
12	73.5	1.4	0
24	73.3	2.6	0.06

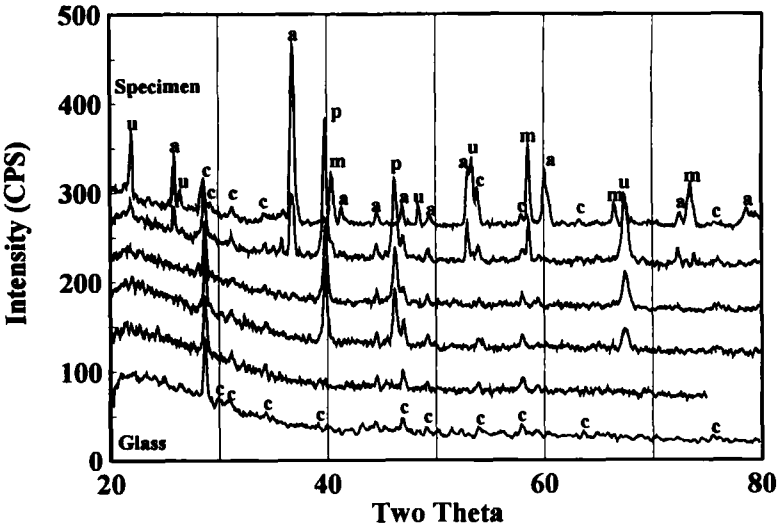

Fig. 5. XRD patterns penetrating from the glass, through the interface, into the molybdenum bulk of a specimen after an exposure of 48 h at 1565°C: a, MoO_2; c, $CaMoO_4$; m, Mo; p, Pt; u, unidentified phase.

peak gradually reduces, then increases in intensity with penetration. Low-intensity peaks corresponding to this phase are still apparent within the interfacial region. The trace corresponding to deepest penetration indicates the presence of MoO_2 and Mo, with minor quantities of $CaMoO_4$. The increase and decrease in the intensity $CaMoO_4$ peak are attributed to the discontinuous composition of the debris in the glass near the interfacial layer. A few small peaks (marked "u" in Fig. 5) could not be matched with any known phases in the JCPDS database. Pt XRD peaks correspond to the Pt wire used in suspending the specimen in the glass melt.

Figure 6 shows the Mo–glass interfacial morphology. An interfacial reaction layer is apparent. From the backscattered image (right-hand side), atomic number contrast of the interfacial layer implies that it was composed of (on average) atomically lighter elements. This was corroborated by the line EDS scan shown in Fig. 7 in which a Mo-depleted (relative to Mo bulk) interfacial region is shown. This corresponds to XRD results showing MoO_2 at penetration depths corresponding to the highest trace in Fig. 5. It is therefore clear that the interfacial layer is MoO_2.

The sharp increase in Si intensity in Fig. 7 near the Mo bulk/interfacial layer interface implies the penetration of glass into the interfacial region. It is interpreted that oxidation of molybdenum caused local expansion and associated compressive stress. These layers thus cracked, allowing penetration of the molten glass.

Our XRD results showed that no $MoO_{3(s)}$ or $MoS_{2(s)}$ was detected within the interfacial region. The latter is in spite of the fact that the glass used in this investigation contained 0.2 wt% of SO_3. Figure 8 shows the Ellingham diagram of various Mo–O_2–Ca equilibria. MoO_2 is clearly favored over MoO_3 since the equilibria line falls above the Richardson line at the testing temperature. This is in agreement with XRD results at the interfacial region. Only near an atmospheric activity of soluble molecular oxygen would MoO_3 be expected to form.

XRD results identified the formation of $CaMoO_4$ at the interfacial region and floating out into the glass. From Fig. 8, reaction between formed MoO_2, calcium oxide, and dissolved oxygen is more favorable than reaction between elemental molybdenum, calcium oxide, and dissolved oxygen. This is

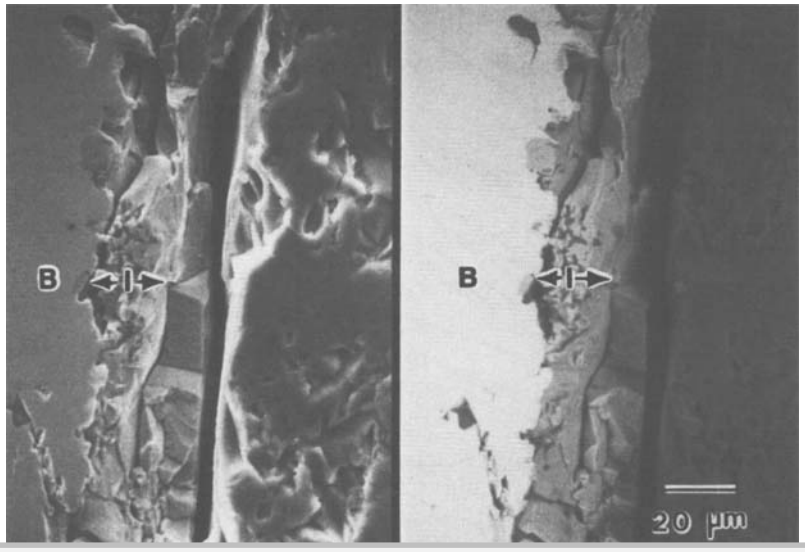

DOCKET ALARM

Explore Litigation Insights

Docket Alarm provides insights to develop a more informed litigation strategy and the peace of mind of knowing you're on top of things.

Real-Time Litigation Alerts

Keep your litigation team up-to-date with **real-time alerts** and advanced team management tools built for the enterprise, all while greatly reducing PACER spend.

Our comprehensive service means we can handle Federal, State, and Administrative courts across the country.

Advanced Docket Research

With over 230 million records, Docket Alarm's cloud-native docket research platform finds what other services can't. Coverage includes Federal, State, plus PTAB, TTAB, ITC and NLRB decisions, all in one place.

Identify arguments that have been successful in the past with full text, pinpoint searching. Link to case law cited within any court document via Fastcase.

Analytics At Your Fingertips

Learn what happened the last time a particular judge, opposing counsel or company faced cases similar to yours.

Advanced out-of-the-box PTAB and TTAB analytics are always at your fingertips.

API

Docket Alarm offers a powerful API (application programming interface) to developers that want to integrate case filings into their apps.

LAW FIRMS
Build custom dashboards for your attorneys and clients with live data direct from the court.

Automate many repetitive legal tasks like conflict checks, document management, and marketing.

FINANCIAL INSTITUTIONS
Litigation and bankruptcy checks for companies and debtors.

E-DISCOVERY AND LEGAL VENDORS
Sync your system to PACER to automate legal marketing.